

A Novel Square-Planar Ni(II) Complex with an Amino—Carboxamido—Dithiolato-Type Ligand as an Active-Site Model of NiSOD

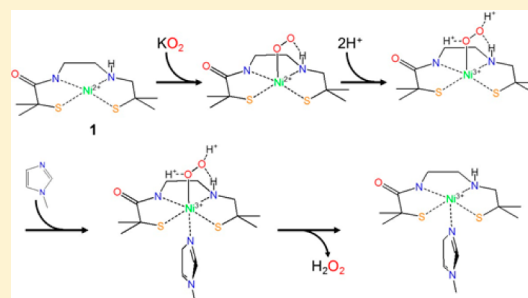
Daisuke Nakane,[†] Yuko Wasada-Tsutsui,[†] Yasuhiro Funahashi,[‡] Tsubasa Hatanaka,[‡] Tomohiro Ozawa,[†] and Hideki Masuda^{*†}

[†]Department of Frontier Materials, Graduate School of Engineering, Nagoya Institute of Technology, Gokiso, Showa, Nagoya 466-8555, Japan

[‡]Department of Chemistry, Graduate School of Science, Osaka University, 1-1 Machikaneyama, Toyonaka, Osaka 560-0043, Japan

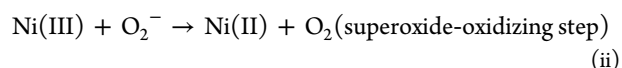
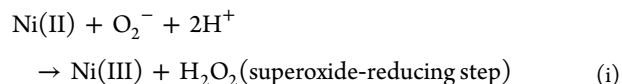
Supporting Information

ABSTRACT: To understand the role of the unique equatorial coordination environment at the active center in nickel superoxide dismutase (NiSOD), we prepared a novel Ni(II) complex with an amino—carboxamido—dithiolato-type square-planar ligand (**1**, [Ni²⁺(L₁)][−]) as a model of the NiSOD active site. Complex **1** has a low-spin square-planar structure in all solvents. Interestingly, the absorption wavelength and $\nu(\text{C}=\text{O})$ stretching vibrations of **1** are affected by solvents. This provides an indication that the carbonyl oxygens participate in hydrogen-bonding interactions with solvents. These interactions are reflected in the redox potentials; the peak potential of an anodic wave (E_{pa}) values of Ni(II)/Ni(III) waves for **1** are shifted to a positive region for solvents with higher acceptor numbers. This indicates that the disproportionation of superoxide anion by NiSOD may be regulated by hydrogen-bonding interactions between the carboxamido carbonyl and electrophilic molecules through fine-tuning of the redox potential for optimal SOD activity. Interestingly, the E_{pa} value of the Ni(III)/Ni(II) couple in **1** in water (+0.303 V vs normal hydrogen electrode (NHE)) is similar to that of NiSOD (+0.290 V vs NHE). We also investigated the superoxide-reducing and -oxidizing reactions of **1**. First, **1** reacts with superoxide to yield the superoxide-bound Ni(II) species (UV-vis: 425, 525, and ~650 nm; electron paramagnetic resonance (EPR) (4 K): $g_{\parallel} = 2.21$, $g_{\perp} = 2.01$; resonance Raman: $\nu(^{16}\text{O}-^{16}\text{O})/\nu(^{18}\text{O}-^{18}\text{O}) = 1020/986 \text{ cm}^{-1}$), which is then oxidized to Ni(III) state only in the presence of both a proton and 1-methylimidazole, as evidenced by EPR spectra. Second, EPR spectra indicate that the oxidized complex of **1** with 1-methylimidazole at the axial site can be reduced by reaction with superoxide. The Ni(III) complex with 1-methylimidazole at the axial site does not participate in any direct interaction with azide anion ($\text{p}K_{\text{a}} 4.65$) added as mimic of superoxide ($\text{p}K_{\text{a}} 4.88$). According to these data, we propose the superoxide disproportionation mechanism in superoxide-reducing and -oxidizing steps of NiSOD in both Ni(II) and Ni(III) states.



INTRODUCTION

The superoxide anion radical (O_2^-) is an unavoidable byproduct of aerobic respiration and causes significant oxidative damage to biomolecules. To prevent biomolecules from damage due to oxidative stress, aerobic organisms have evolved redox-active metalloenzymes known as superoxide dismutases (SODs). SODs catalyze the disproportionation of superoxide anion to hydrogen peroxide (H_2O_2) and molecular dioxygen (O_2) through reduction and oxidation processes.^{1,2} The Ni-containing superoxide dismutase (NiSOD), which has been discovered from *Streptomyces*^{3,4} and the genome of cyanobacteria,⁵ is a relatively novel type of SOD. This enzyme catalyzes the disproportionation of superoxide anion through the following reactions:

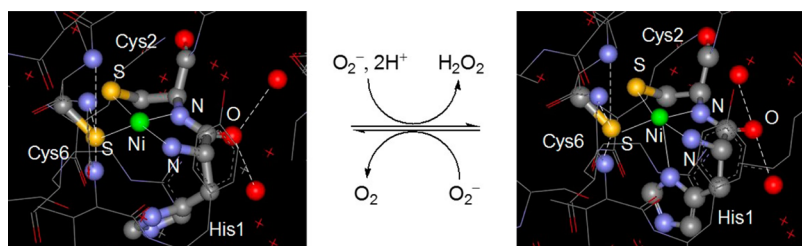


The structures of NiSOD in both the Ni(II) and Ni(III) states have been revealed by X-ray crystallography. In the reduced Ni(II) state, the active center contains a square-planar Ni(II) ion coordinated by an amino group of the terminal histidine, a carboxamido nitrogen atom of the peptide backbone, and two thiolato sulfur atoms of cysteine residues in the equatorial plane.^{6,7} In the Ni(III) state, it is additionally coordinated by a histidyl imidazole at the axial position of the

Received: October 15, 2013

Published: June 18, 2014



Scheme 1. Superoxide Disproportionation Mechanism and Hydrogen Bonds in the Vicinity of the NiSOD (from *S. lividans* TK24) Active Center

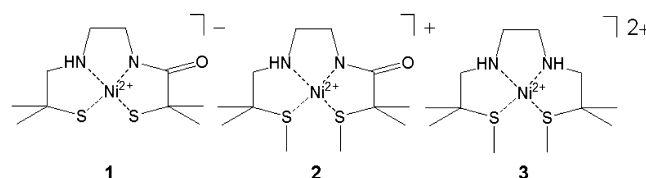
metal center.⁶ In addition to these first coordination environments, in both cases, the second coordination sphere includes two water molecules that interact with the oxygen atom of the carboxamido group of the peptide backbone through a hydrogen bond. The thiolato sulfur of Cys6 also interacts with NH protons of the peptide backbone (Scheme 1).^{6,7}

The first and second coordination spheres of the NiSOD active site therefore play an important role in the disproportionation of the superoxide anion. The effect of the first coordination sphere has been characterized. From comparison studies of the redox potentials for the Ni(II)/(III) process using model compounds of the NiSOD active site with an N_2S_2 -type square-planar structure, it was suggested that the amino–carboxamido–dithiolato-type coordination of the NiSOD active site provides a Ni(II)/(III) redox potential appropriate for dismutation of the superoxide anion.^{8–11} An electrochemical study suggested that axial coordination of histidyl imidazole stabilizes the Ni(III) state for promotion of the superoxide reduction process.^{12–15} In addition, a theoretical study has suggested that in the superoxide-oxidizing step, the axial coordination to the Ni(III) ion causes destabilization of the d_{z^2} character of the singly occupied molecular orbital (SOMO). This supports the Ni(III)-based electron transfer from superoxide to the active metal center.¹²

Second, we focused on the effect of the second coordination sphere on SOD activity. Although a large number of investigations of the first coordination environment have been undertaken, there have been few studies on the second coordination environment. Shearer et al. focused on the hydrogen bond in the second coordination sphere.¹⁶ The hydrogen-bonding interactions between the histidyl imidazole of His1 and the carboxyl group of Glu17 were investigated using an oligometallopeptide, and it was concluded that the hydrogen bond tunes the Lewis acidity of metal center for SOD function.¹⁶ Harrop et al. investigated the hydrogen bond between the thiolato sulfur of Cys6 and a NH proton of the peptide backbone using a Ni(II) complex with a N_2S_2 -type square-planar structure as a model of the NiSOD active site and investigated the effects of a hydrogen bond in the vicinity of the secondary coordination sphere by changing the substituents of functional groups.¹⁷ It was suggested that the hydrogen bond prevents oxidation of the thiolato groups.¹⁷ However, there have been no reports focused on direct investigation of hydrogen-bonding effects, which are observed between carboxamido oxygen and water molecules.

Elucidation of the disproportionation mechanism of superoxide anion by NiSOD is a fascinating problem. We have previously described two N_2S_2 -type square-planar Ni(II) complexes with amino–carboxamido–dithioether- (L_2) and diamino–dithioether-type ligands (L_3) (2, 3, Chart 1), determined their crystal structures, and characterized their

Chart 1. Ni(II) Complexes $[Ni^{2+}(L_1)]^-$ (1), $[Ni^{2+}(L_2)]^+$ (2), and $[Ni^{2+}(L_3)]^{2+}$ (3) Prepared As Models of the NiSOD Active Center



spectral/electrochemical properties and reactivities with superoxide anion. Both complexes are oxidized to the Ni(III) state by reaction with potassium superoxide (KO_2), which corresponds to the superoxide reduction step of NiSOD. The structural changes occurring during the oxidation have been described.^{18,19} Although a few theoretical studies have been published on the mechanism of superoxide dismutation by NiSOD,^{12,20–25} there have been fewer experimental investigations.^{16,17,26–33}

In this study, we describe a novel square-planar Ni(II) complex 1 with an amino–carboxamido–dithiolato-type ligand (L_1) as a model of the active site of NiSOD. The coordination environment of the Ni(II) ion of complex 1 is similar to that of the NiSOD active site. We investigated the following three properties of the complex: (i) the relationship between the redox potential for the Ni(II)/(III) process and the interactions between the carboxamido oxygen/thiolato sulfurs with solvents; (ii) the coordination behavior of external ligands such as imidazole derivatives and azide anion in the Ni(II) and Ni(III) states; and (iii) the reactivities between the Ni(II)/Ni(III) complexes and superoxide anion in the presence/absence of an imidazole derivative. The results of these investigations led us to propose a mechanism for superoxide dismutation by NiSOD.

EXPERIMENTAL SECTION

Materials. (n -Bu)₄NBF₄ was purchased from Tokyo Chemical Industry. All other reagents and solvents were obtained from Wako Pure Chemical Industry, Ltd. and were of the highest grade available. 2-Benzylmercapto-2-methylpropanoic acid and 2-chloro-1-methylpyridinium iodide were prepared by previously reported methods.^{34,35}

Preparations of Ni(II) Complexes 2 and 3. Ni(II) complexes of *N*-(2-methylmercapto-2-methylpropanoyl)-*N'*-(2-methylmercapto-2-methylpropyl)-1,2-diaminoethane (2) and of *N,N'*-bis(2-methylmercapto-2-methylpropyl)-1,2-diaminoethane (3) were prepared by previously reported methods.^{18,19,36}

Preparation of Ligand. Synthetic scheme of the Ni(II) complex 1 is summarized in Supporting Information, Scheme S1.

N-(2-Benzylmercapto-2-methylpropanoyl)-1,2-diaminoethane. Triethylamine (2.0 g, 19 mmol) and 2-benzylmercapto-2-methylpropanoic acid (4.0 g, 19 mmol) were dissolved in MeCN (100 mL). To the solution was added 2-chloro-1-methylpyridinium iodide (4.8 g,

19 mmol), and the solution was stirred for 1 h. This solution was added dropwise into 1,2-diaminoethane (20 mL) and stirred overnight. The solvent and unreacted 1,2-diaminoethane were removed *in vacuo* to afford an oily orange residue. The oil was dissolved into an alkaline aqueous solution at pH 12 and was extracted three times with EtOAc (50 mL). The EtOAc layer was washed with saturated NaCl aqueous solution and dried with anhydrous sodium sulfate (Na_2SO_4). The solvent was removed under reduced pressure to afford *N*-(2-benzylmercapto-2-methylpropanoyl)-1,2-diaminoethane as a clear oil. (Yield 3.1 g, 63%). NMR: $\delta(\text{CDCl}_3, 300 \text{ MHz})$: 1.56 (s, 6H), 2.78 (t, 2H), 3.20 (dd, 2H), 3.76 (s, 2H), 7.29 (m, 5 + 1H).

N-(2-Benzylmercapto-2-methylpropyl)-1,2-diaminoethane. Ethereal trifluoroboron solution (12.8 g, 90 mmol) was added to the tetrahydrofuran (THF) solution (50 mL) of NaBH_4 (1.7 g, 45 mmol), and the solution was stirred for 10 min. This solution was added to a THF solution (150 mL) of *N*-(2-benzylmercapto-2-methylpropanoyl)-1,2-diaminoethane (3.1 g, 12.3 mmol). The resulting mixed solution was refluxed for 20 h. Small volumes of MeOH were added to the solution to decompose the remaining B_2H_6 . After addition of H_2O (100 mL) to the solution, the organic solvent was evaporated. The resulting aqueous solution was extracted three times with EtOAc (50 mL) at pH 12. The EtOAc layer was dried with anhydrous Na_2SO_4 after treatment with saturated NaCl solution. EtOAc was removed under reduced pressure to afford *N*-(2-benzylmercapto-2-methylpropyl)-1,2-diaminoethane as a clear oil. (Yield 2.0 g, 70%). NMR: $\delta(\text{CDCl}_3, 300 \text{ MHz})$: 1.34 (s, 6H), 1.86 (br, 2H), 2.51 (s, 2H), 2.54 (dd, 2H), 2.73 (t, 2H), 3.70 (s, 2H), 7.32 (m, 5H).

N-(2-Benzylmercapto-2-methylpropanoyl)-*N'*-(2-benzylmercapto-2-methylpropyl)-1,2-diaminoethane. Triethylamine (0.88 g, 8.35 mmol) and 2-benzylmercapto-2-methylpropanoic acid (1.77 g, 8.35 mmol) were dissolved in MeCN (100 mL). 2-Chloro-1-methylpyridinium iodide (2.1 g, 8.35 mmol) was added, and the solution was stirred for 1 h. *N*-(2-benzylmercapto-2-methylpropyl)-1,2-diaminoethane in MeCN (50 mL) was introduced, and the solution was stirred overnight. The solvent was removed under reduced pressure to afford an oily yellow material. The oil was extracted three times with Et_2O (50 mL) at pH 12. The organic layer was washed with saturated NaCl and dried with anhydrous Na_2SO_4 . The solvent was removed under reduced pressure to afford *N*-(2-benzylmercapto-2-methylpropanoyl)-*N'*-(2-benzylmercapto-2-methylpropyl)-1,2-diaminoethane as a clear oil. The oil was purified by column chromatography with a 20:1 mixture of $\text{CHCl}_3/\text{MeOH}$. (Yield 2.6 g, 69%). NMR: $\delta(\text{CDCl}_3, 300 \text{ MHz})$: 1.32 (s, 6H), 1.53 (s, 6H), 2.47 (s, 2H), 2.54 (t, 2H), 3.17 (dd, 2H), 3.67 (s, 2H), 3.73 (s, 2H), 7.21–7.35 (m, 10H), 7.37 (br, 1H).

N-(2-Mercapto-2-methylpropanoyl)-*N'*-(2-mercapto-2-methylpropyl)-1,2-diaminoethane (**1**). *N*-(2-benzylmercapto-2-methylpropanoyl)-*N'*-(2-benzylmercapto-2-methylpropyl)-1,2-diaminoethane (2.6 g, 5.8 mmol) was dissolved in dry THF (5 mL). Na (1 g, 43 mmol) was added to the solution after addition of liquid ammonia (100 mL) to the solution at -78°C . After stirring for 30 min, NH_4Cl was added until the blue color of the solution completely disappeared. The ammonia was removed at room temperature, and H_2O (50 mL) was added to the residue under an Ar atmosphere. After the solution was washed with Et_2O (50 mL) at pH 12, the resulting solution was extracted three times with EtOAc (50 mL) at pH 8. The EtOAc layer was dried with anhydrous Na_2SO_4 after treatment with saturated NaCl solution. The organic solvent was removed to afford *N*-(2-mercapto-2-methylpropanoyl)-*N'*-(2-mercapto-2-methylpropyl)-1,2-diaminoethane as a clear oil. (Yield 1.25 g, 83%). NMR: $\delta(\text{CDCl}_3, 300 \text{ MHz})$: 1.38 (s, 6H), 1.60 (s, 6H), 2.62 (s, 2H), 2.85 (t, 2H), 3.35 (dd, 2H), 7.46 (br, 1H).

Preparation of Ni(II) Complex 1. The synthesis of complex **1** was conducted under an Ar atmosphere. *N*-(2-mercapto-2-methylpropanoyl)-*N'*-(2-mercapto-2-methylpropyl)-1,2-diaminoethane (1.25 g, 4.98 mmol) in dimethylformamide (DMF) (10 mL) was deprotonated with NaH (0.35 g, 15.1 mmol). When $\text{NiCl}_2 \cdot 6\text{H}_2\text{O}$ (0.71 g, 3.0 mmol) dissolved in DMF (5 mL) was dropped into the solution, the color changed from green to dark red. After stirring overnight, an insoluble white precipitate was filtered out, and removal of solvent from this filtrate *in vacuo* produced the crude product as a dark red slurry. The

slurry was dissolved in MeCN (10 mL), and insoluble impurities were filtered out. To this clear MeCN solution was added hexane (30 mL), to produce a dark red precipitate. The precipitate was washed with acetone to give an orange powder. The powder was recrystallized from MeCN solution with slow diffusion of Et_2O to give red crystals of **1**. (Yield 0.41 g, 42%). Electrospray ionization mass spectrometry (ESI-MS) (m/z): $[\text{M}]^-$ Calcd for $\text{C}_{10}\text{H}_{19}\text{N}_2\text{S}_2\text{ONi}$, 305.0. Found. 305.1. Elemental anal. Calcd for $\text{C}_{10}\text{H}_{19}\text{N}_2\text{S}_2\text{ONiNa} \cdot 0.5\text{Et}_2\text{O}$, C: 39.36, H: 6.61, N: 7.65, S: 17.51, Found, C: 39.08, H: 6.35, N: 7.92, S: 17.40%. NMR: $\delta(\text{D}_2\text{O}, 600 \text{ MHz})$: 1.24 (s, 3H), 1.27 (s, 3H), 1.32 (s, 3H), 1.39 (s, 3H), 2.56 (d, 1H), 2.62 (d, 1H), 2.76 (d, 1H), 2.88 (d, 2H), 3.25 (d, 1H).

Physicochemical Measurements. Electronic absorption spectra were measured using a JASCO U-best V-550 spectrometer. The temperature was tuned by using UNISOKU UnispeKs. ^1H NMR spectra were measured using a Varian Gemini-300 NMR spectrometer. Cyclic voltammetry measurements were performed using an Electrochemical Analyzer Model 600A (ALS/CH Instruments). Glassy carbon, Ag/Ag $^+$ (in organic solvents), Ag/AgCl (in water), and Pt-wire electrodes were used as working, reference, and counter electrodes, respectively. (*n*-Bu) $_4$ NBF $_4$ (0.1 M, in organic solvents) or NaClO $_4$ (0.1 M, in water) was employed as an electrolyte at room temperature under an Ar atmosphere. All potentials are reported relative to the normal hydrogen electrode (NHE) using Cp $_2$ Fe/Cp $_2$ Fe $^+$ (in organic solvents) or Ag/AgCl electrode (in water) as the standard.³⁷ EPR spectra were measured using a JEOL JES-RE1X with quartz tube. All samples were prepared as 5 mM solutions in a 4:1 mixture of acetone/DMF at -78°C and measured at -196°C . The accurate magnetic fields are calibrated by using NMR field meter JEOL ES-FC5. EPR spectrum of the reaction product of complex **1** with KO $_2$ was measured also at 4 K by using JEOL JES-TE300. IR spectra were measured using a JASCO FT/IR-4200 spectrometer with a CaF $_2$ cell. Samples for IR spectroscopy were prepared as 0.1 M solutions of complexes. Convenient magnetic susceptibility measurements were carried out for solution samples using the Evans method.³⁸ Resonance Raman (rR) spectra were measured by using a JASCO NKS-1000 spectrometer with an NMR tube. Samples were prepared as 20 mM solution of **1** in DMF and reacted with the same equivalents of KO $_2$ at -50°C . A laser (532 nm Ar, 70 mW) was used for excitation.

X-ray Crystallography. A single crystal of complex **1** was mounted on a glass fiber. X-ray measurements were made on a Rigaku Mercury CCD area detector with graphite monochromated Mo K α radiation. The data were collected at a temperature of $-100 \pm 1^\circ\text{C}$ to a maximum 2θ value of 20.0° . A total of 1200 oscillation images were collected. The structure was solved by direct methods³⁹ and expanded using Fourier techniques.⁴⁰ The non-hydrogen atoms were refined anisotropically. Hydrogen atoms were refined isotropically using the riding model.

Theoretical Calculations. All geometries of superoxide-Ni(II) complexes in the singlet ($S = 1/2$) state were optimized at the density functional theory (DFT) level using GGA exchange functional OPTX^{41,42} in combination with the correlation functional PBE (OPBE).⁴³ DFT calculations with pure functionals, such as OPBE,⁴⁷ give reasonable binding energies of CO, NO, and O $_2$ for Fe complexes bound with donor atoms of the conjugated ligand system.^{44–46} The 6-31G(d) basis set³⁶ was used for all atoms except for the Ni atom that was used in the 6-311G basis set.^{48,49} Two diffuse p functions were added to the basis set for Ni; these are the functions optimized by Wachters and multiplied by 1.5.⁴⁸ The diffuse functions (6-31+G(d)) were added for N, O, and S atoms.⁵⁰ For the π^* orbitals of superoxide, we selected two molecular orbitals (MOs) that have the largest MO coefficients among all of the occupied α -orbitals of the O $_2^-$ molecule. All calculations were carried out with the Gaussian 09 package⁵¹ on the Fujitsu HX600 at the Nagoya University Information Technology Center. The contour maps and isosurfaces of the MOs were drawn using MOPLOT and MOVIEW programs.⁵²

RESULTS AND DISCUSSION

Design and Preparation of Ni(II) Complex 1 as a Model of the NiSOD Active Center. To mimic the coordination structure of the NiSOD active site, we designed a square-planar Ni(II) complex **1** with an amino-carboxamido-dithiolato-type ligand (L_1) as the NiSOD structural model. This compound is composed of the same first coordination environment as the NiSOD active site and includes one amine nitrogen, one carboxamido nitrogen, and two thiolato sulfurs. Complex **1** was prepared by reaction of $NiCl_2 \cdot 6H_2O$ with deprotonated L_1 ligand in DMF. The absorption maxima in the UV-vis spectrum of complex **1** (438–449 nm, $227\text{--}357\text{ M}^{-1}\text{ cm}^{-1}$) are similar to those of Ni(II) complexes $[Ni^{2+}(BEAAM)]^-$ (483 nm, $290\text{ M}^{-1}\text{ cm}^{-1}$)⁸ and $[Ni^{2+}(HL_2)]^-$ (449 nm, $340\text{ M}^{-1}\text{ cm}^{-1}$),¹⁰ which have an amino-carboxamido-dithiolato framework, and those of native reduced NiSOD (450 nm).¹² Fortunately, we obtained a single crystal suitable for X-ray structure analysis from MeCN/Et₂O solution. According to the X-ray analysis, eight Ni(II) complexes, eight sodium cations, and four diethyl ether molecules are included in the unit cell. The crystal structure of complex **1** is shown in Figure 1 together with its selected bond

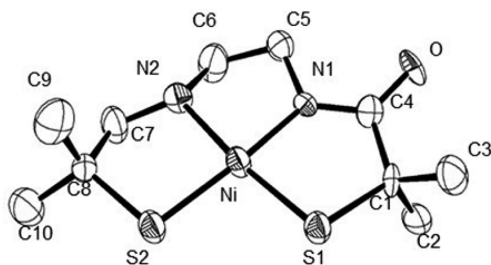


Figure 1. ORTEP drawing of the anion moiety of **1** with thermal ellipsoids drawn at 50% probability. The hydrogen atoms, counter-cations (sodium), and diethyl ether molecules are omitted for clarity. Selected bond lengths (Å) and angles (deg): Ni–N(1) = 1.865(5), Ni–N(2) = 1.923(5), Ni–S(1) = 2.1450(19), Ni–S(2) = 2.1702(18), N(1)–Ni–S(2) = 175.88(16), N(2)–Ni–S(1) = 173.56(14), N(1)–Ni–S(1) = 88.19(16), S(1)–Ni–S(2) = 95.93(7), N(2)–Ni–S(2) = 89.84(15), N(1)–Ni–N(2) = 86.1(2).

lengths and angles. Complex **1** has a coordination environment similar to the active center of NiSOD, as expected from the design concept. The Ni atom forms a square-planar structure coordinated with one carboxamido nitrogen, one amino nitrogen, and two thiolato sulfurs in the equatorial plane. The metal–ligand bond lengths in complex **1** are similar to those of the NiSOD active site; for complex **1**, the bond lengths are Ni–N(1)^{amide} = 1.865(5) Å, Ni–N(2)^{amine} = 1.923(5) Å, Ni–S(1) = 2.1450(19) Å, and Ni–S(2) = 2.1702(18) Å; for NiSOD,

they are Ni–N^{amide} = 1.91 ± 0.03 Å, Ni–N^{amine} = 2.02 ± 0.10 Å, Ni–S = 2.16 ± 0.02, 2.19 ± 0.02 Å.⁶ These bond lengths are quite similar to those of $[Ni^{2+}(BEAAM)]^-$ (Ni–N(1)^{amide} = 1.858(6) Å, Ni–N(2)^{amine} = 1.989(7) Å, Ni–S(1) = 2.137(2) Å, and Ni–S(2) = 2.177(2) Å)⁸ and those of $[Ni^{2+}(HL_2)]^-$ (Ni–N(1)^{amide} = 1.862(2) Å, Ni–N(2)^{amine} = 1.937(3) Å, Ni–S(1) = 2.1671(8) Å, and Ni–S(2) = 2.1711(7) Å).¹⁰ The bond lengths of **1** and Ni(II) complexes are slightly shorter than those of native NiSOD, as a result of the strong coordination environment provided by the three five-membered chelate rings of complex **1**. In complex **1**, the Ni–N(1)^{amide} bond (1.865(5) Å) is significantly shorter than the Ni–N^{amine} bond (1.923(5) Å), which is found in the N₂S₂-type square-planar Ni(II) complexes with amino-carboxamido-dithiolato framework.^{8–10,18} This is explained in terms of the stronger donor ability of an amide nitrogen relative to an amine nitrogen. This tendency is consistent with the square-planar Ni(II) complexes with N₂S₂-type ligands with three five-membered chelate rings, which have been reported previously.^{8–10,53} The slightly longer Ni–S bond (2.1702(18) Å) trans to the carboxamido nitrogen in comparison with the Ni–S bond (2.1450(19) Å) trans to the amine nitrogen is due to the stronger trans influence of the former relative to the latter. Because of delocalization of the negative charge of the carboxamido group onto the ligand, the C(4)–O (1.271(7) Å) and C(4)–N(1) (1.313(7) Å) bond lengths are in the intermediate range between single and double bonds.

Structures of Ni(II) Complexes 1, 2, and 3 in Solutions.

As described above, complexes **1** and **2** produce intense bands at 438–450 nm and ~435 nm in all solvents, respectively (Table 1, Supporting Information, Figure S1). These bands are assigned to a mixture of the ligand-to-metal charge-transfer (LMCT) band of thiolato S[−] to Ni(II) dπ and d–d transitions of the Ni(II) ion that originate from low-spin square-planar Ni(II) complexes with N₂S₂-type ligands.^{8–10,53} The absorption spectra of complex **3** have three weak absorption maxima at 350–400 nm, 530–650 nm, and 820–900 nm. These spectra, which are typical for a high-spin Ni(II) species in MeCN, dimethyl sulfoxide (DMSO), and DMF, exhibit an absorption maximum typical of a low-spin Ni(II) species at approximately 475 nm in acetone, propylene carbonate (PC), EtOH, and MeOH (Table 1). These characteristics also indicate that coordination of the carboxamido nitrogen or thiolato sulfurs to the metal center for **1** and **2** promotes a strong binding to the d_{x²−y²} orbital of the metal ion to induce the formation of a low-spin Ni(II) species. These solution structures are also supported by the magnetic susceptibility values of Ni(II) complexes **1**, **2**, and **3**, measured in several solvents using the Evans method.²⁷ Complexes **1** and **2** exhibit diamagnetic properties in all solvents used here (DMA, acetone, DMF,

Table 1. Electronic Absorption Spectral Data and Magnetic Properties of Ni(II) Complexes 1, 2, and 3 in Several Solvents

	DMA	DMF	MeCN	DMSO	acetone	PC	EtOH	MeOH	water
1	448 (357)	449 (343)	445 (334)	446 (339)			441 (285)	441 (258)	438 (227)
2		435 (292)	436 (332)	435 (247)	436 (390)		435 (308)	436 (301)	439 (308)
3		379 (30)	352 (50)	394 (16)					
		614 (13)	535 (20)	642 (7)	478 (257)	476 (217)		475 (213)	
		−900 (24)	826 (30)	−900 (15)					
			paramagnetic				diamagnetic		

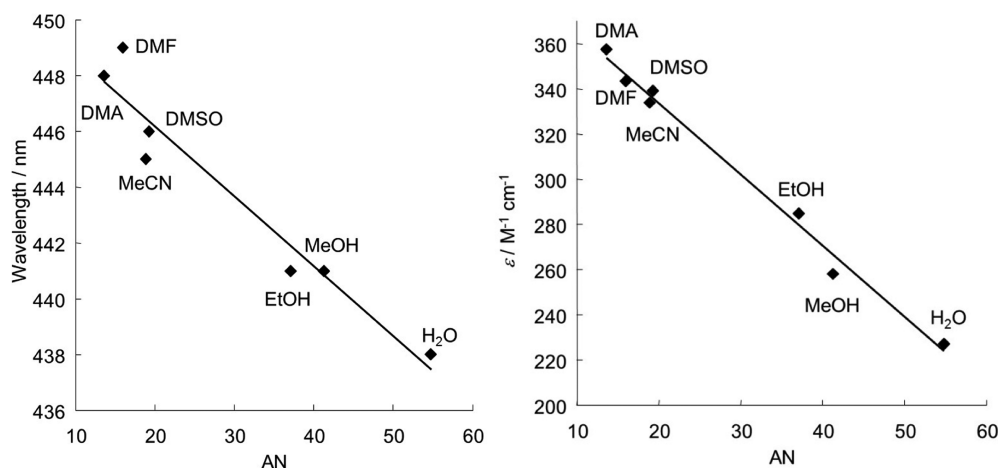


Figure 2. Relationships between the maxima of the electronic absorption bands of Ni(II) complex **1** at 440 nm (left) and the solvent acceptor numbers (AN), and between their molar extinction coefficients (right) and the solvent AN.

Table 2. Relationships between $\nu(\text{C}=\text{O})$ Values of **1** and **2** and Acceptor Numbers of Solvents

solvent	acetone	DMA	DMF	MeCN	DMSO	EtOH	MeOH	water
acceptor number	12.5	13.6	16.0	18.9	19.3	37.1	41.3	54.8
$\nu(\text{C}=\text{O}), \text{cm}^{-1}$								
1		1573	1572	1573	1569	1562	1560	1554
2	1624		1619	1618	1613		1586	1576

MeCN, DMSO, MeOH, EtOH, and water). On the other hand, complex **3** was found to have paramagnetic character in MeCN ($\mu_{\text{eff}} = 2.7 \mu_{\text{B}}$), DMSO ($\mu_{\text{eff}} = 2.7 \mu_{\text{B}}$), and DMF ($\mu_{\text{eff}} = 2.7 \mu_{\text{B}}$) and diamagnetic character in acetone, PC, EtOH, and MeOH. The magnetic properties of these Ni(II) complexes suggest that complex **3** is in a low-spin state ($S = 0$) in PC, EtOH, and MeOH and in a high-spin state ($S = 1$) in MeCN, DMSO, and DMF, while complexes **1** and **2** are in a low-spin state in all solvents examined. These findings indicate that in MeCN, DMSO, and DMF, complex **3** coordinates to the solvent molecules to form a high-spin five- or six-coordinate species, whereas in the other solvents examined, it is not bound by any solvent molecules. These findings indicate that the square-planar structures of Ni(II) complexes **1** and **2** are stabilized by the strong electron-donor characteristics of the carboxamido nitrogen and/or thiolato sulfurs and are not affected by the donating abilities of solvents. These findings also indicate that the magnetic property of complex **3** is controlled by solvents. In addition to these magnetic properties in various solvents, complex **1** has absorption maxima with smaller molar absorption coefficients in the higher-energy region in the solvents with a larger acceptor number (AN, a parameter of electrophilicity),⁵⁴ as shown in Table 1 and Figure 2, while the absorption maxima of complex **2** do not undergo such a shift. These shifts appear to be due to an electrostatic interaction between the thiolato S atoms of complex **1** and solvent molecules.

Solvent-Dependent IR Spectroscopic Behavior of the Carboxamido Carbonyl Group of Complexes 1 and 2. To investigate the effect of hydrogen-bonding interactions between the carboxamido nitrogen and water molecules in NiSOD, which are found in the second coordination sphere of the active center, the C=O stretching frequencies of the carbonyl groups, $\nu(\text{C}=\text{O})$, for complexes **1** and **2** were measured in several different solvents using IR spectroscopy. As expected, these complexes showed a significant solvent effect, which may be related to the hydrogen-bonding interaction between the

carboxamido carbonyl oxygen and water molecules in the NiSOD active site. Therefore, we examined the relationships between the $\nu(\text{C}=\text{O})$ values and the acceptor numbers of solvents. As shown in Table 2, Figure 3, and Supporting

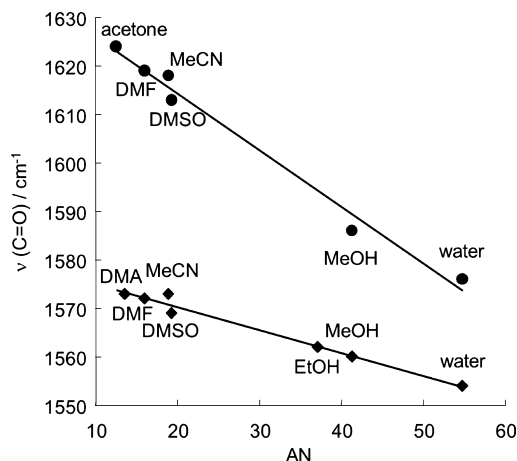


Figure 3. Relationships between $\nu(\text{C}=\text{O})$ values of **1** (◆) and **2** (●) and acceptor numbers of solvents.

Information, Figure S2, the $\nu(\text{C}=\text{O})$ values of complexes **1** and **2** are strongly affected by the ANs of solvents, and the $\nu(\text{C}=\text{O})$ values shift to a lower-energy region in solvents with larger ANs. These findings suggest the existence of a strong nucleophilic interaction between the carboxamido oxygen atom of complexes **1** and **2** and solvent molecules, which causes the carboxamido carbonyl group to be attracted to electrophilic solvents. Thus, we propose that the hydrogen-bonding interaction between the carboxamido carbonyl oxygen and water molecules at the active center of NiSOD may play an important role for tuning redox potential of Ni(II)/(III) process for the function of SOD.

Table 3. Redox Potentials of Ni(II) Complexes 1, 2, and 3 in Several Solvents

complex	solvent acceptor number	acetone 12.5	DMA 13.6	DMF 16.0	PC 18.3	MeCN 18.9	DMSO 19.3	EtOH 37.1	MeOH 41.3	water 54.8
1	E_{pa}^a , V		-0.181	-0.156		-0.114	-0.103	0.041	0.125	0.303
	E_{pc} , V		-0.253	-0.230		-0.225	-0.181	-0.730	-0.578	-0.607
	ΔE , mV		72	74		111	78	771	703	910
	$\Delta E_{1/2}$, V		-0.217	-0.193		-0.170	-0.142			
2	E_{pa} , V	-1.093		-1.095		-1.064	-1.070	-0.951	-0.935	-0.849
	E_{pc} , V	-1.160		-1.169		-1.132	-1.144	-1.045	-1.013	-0.925
	ΔE , mV	67		74		68	74	94	78	76
	$\Delta E_{1/2}$, V	-1.127		-1.132		-1.098	-1.107	-0.998	-0.974	-0.887
3	E_{pa} , V	-0.611		-0.811	-0.557	-0.631	-0.807	-0.547	-0.539	
	E_{pc} , V	-0.676		-0.912	-0.657	-0.726	-0.948	-0.620	-0.607	
	ΔE , mV	65		101	100	95	141	73	68	
	$\Delta E_{1/2}$, V	-0.644		(-0.862) ^b	-0.607	(-0.679) ^b	(-0.878) ^b	-0.584	-0.573	

^aAll potentials are converted to the NHE scale and referenced to a Cp_2Fe/Cp_2Fe^+ standard ($E_{1/2} = 0.40$ V). Electrochemical potentials were measured vs Ag/Ag^+ (organic solvent) and a $Ag/AgCl$ (in water) reference electrode using 0.1 M $n-Bu_4NBF_4$ as the electrolyte and glassy carbon as the working electrode. ^bComplex 3 showed paramagnetic properties in these solvents.

Electrochemical Properties of Complexes 1, 2, and 3.

The above-mentioned findings lead us to expect that the lower-energy shifts of $\nu(C=O)$ values of the carboxamido carbonyl groups for complexes 1 and 2 have a significant influence on the electron density of the metal. We therefore studied the electrochemical properties of Ni(II) complexes 1, 2, and 3 in selected solvents.

Complex 1, which has amino-carboxamido-dithiolato-type square-planar coordination, has a reversible redox couple corresponding to a Ni(II)/(III) process in DMA, DMF, MeCN, and DMSO and exhibits irreversible waves with a large separation in EtOH, MeOH, and H₂O (Table 3 and Supporting Information, Figure S3). The waves are due not to the oxidation process of sulfurs but to the Ni(II)/(III) process of the nickel center because, if the waves were an oxidation wave of sulfur, their reduction waves should not be detected. Also, other irreversible waves without reduction wave, which are assignable to sulfur oxidation, were observed at more positive potentials. Furthermore, these redox waves assigned to the Ni(II)/(III) process did not show any changes for cycling of the potentials. So, we considered that the large peak separations were due to structural changes around the metal center upon oxidation. The large separation of the Ni(II)/(III) process for 1 observed in protonic solvents may be explained in terms of the coordination of solvent molecule(s) to the Ni(III) center of complex 1. Interestingly, the E_{pa} value of the Ni(II)/(III) process for complex 1 observed in water (+0.303 V) is fairly similar to that of native NiSOD (+0.290 V).⁵⁵ This finding may indicate that fine-tuning of the Ni(II)/(III) redox potential of the metal center in NiSOD is important for SOD function.

Nickel complexes with amino-carboxamido-dithioether- and diamino-dithioether-type ligands, namely, 2 and 3, exhibit a reversible redox couple corresponding to the Ni(II)/(III) process at +1.26 V (vs NHE) and +1.71 V (vs NHE) only in specific solvents (CH₂Cl₂ for 2 and acetone for 3), respectively.^{18,19} The redox potentials of the Ni(II)/(III) process for 2 and 3 are significantly higher than that of 1 in all of the solvents examined. These findings are explained as follows: the charges of the ligands for complexes 2 and 3 are -1 and neutral, respectively, while that for complex 1, which is composed of strong donor atoms of carboxamido and thiolato groups, is -3. The lower redox potential of complex 1

compared with those of 2 and 3 is desirable for SOD function, because the redox potentials required for SOD activity should be in the range from -0.16 to +0.89 V vs NHE.¹¹

In other solvents, complexes 2 and 3 exhibit irreversible redox waves or higher potential values within the potential windows of solvents. Because of the irreversible waves and higher potentials of the Ni(II)/(III) redox process, we could not compare the solvent dependency of this process. On the other hand, complexes 2 and 3 each exhibit a reversible redox couple corresponding to the Ni(I)/(II) process in all of the solvents examined.

As shown in Table 3, complex 2 has a lower Ni(I)/(II) redox potential than that of complex 3. Considering the strong donor character of the deprotonated carboxamido nitrogen of complex 2, this corresponds to the expected electrochemical behavior. The redox potentials for the Ni(I)/(II) process of complex 3 in MeCN, DMSO, and DMF fall into a wide range between -0.68 and -0.88 V vs NHE, and those in acetone, PC, EtOH, and MeOH are detected in a narrow range from -0.57 to -0.64 V vs NHE. As described above, complex 3 is in the low-spin state in acetone, PC, EtOH, and MeOH and adopts the high-spin state in MeCN, DMSO, and DMF, while complex 2 is in the low-spin state in all of the solvents examined. Here, to exclude the influence of electrochemical properties according to the different spin states, we compare and discuss only the redox potentials of complexes 2 and 3 in the low-spin state.

Under these conditions, as shown in Figure 4, the E_{pa} values corresponding to the Ni(II)/(III) process of complex 1 with amino-carboxamido-dithiolato-type coordination have a linear relationship with the ANs of the solvents. The E_{pa} values of 1 are strongly affected by ANs of solvents (11.2 mV/AN), while the redox potentials of complex 2 with the amino-carboxamido-dithioether-type ligand were less affected by the ANs of solvents (5.9 mV/AN) in MeCN, DMSO, DMF, acetone, EtOH, and H₂O, although these potentials of complex 2 were found to have a linear relationship with the ANs of solvents. On the other hand, the redox potentials of complex 3 are least affected by ANs (2.1 mV/AN) in acetone, PC, EtOH, and MeOH. The difference in these slopes reveals that the redox potentials of these complexes are affected by an attractive interaction with solvent molecules. Considering the differences in the structures of these complexes, it is clear that the carbonyl and thiolato groups contribute to the attractive interaction.

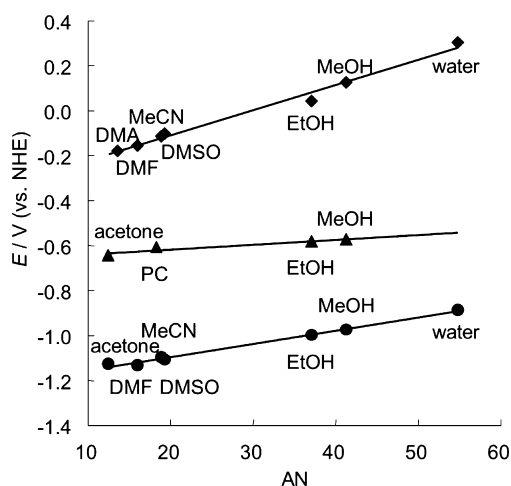


Figure 4. Relationships of E_{pa} (1, ◆) for Ni(II)/(III) and $E_{1/2}$ (2, ●, ▲) for Ni(I)/(II) for acceptor numbers of solvents.

We determined the relationship between the $\nu(\text{C}=\text{O})$ values and redox potentials of 1 and 2 in selected solvents. As seen in Table 4 and Figure 5, the redox potentials of 1 and 2 are shifted to a positive region with a decrease in the $\nu(\text{C}=\text{O})$ values. This indicates that the strong attractive interaction of the carboxamido carbonyl group with solvent molecules weakens the donation of the carboxamido nitrogen, and this causes the redox potential to shift to the positive region. Clearly, the interaction between the carboxamido carbonyl oxygen atoms of complexes 1 and 2 and the solvent molecules significantly affects the redox potential of the metal ion. In the relationship between $\nu(\text{C}=\text{O})$ and E_{pa} , complex 1 has a larger slope than complex 2, as shown in Table 4 and Figure 5. These findings also suggest the presence of the effective attractive interaction between thiolato sulfurs and solvent molecules, in addition to the interaction between carboxamido carbonyl oxygen and solvent molecules (see Table 5).

These findings provide strong evidence that, in addition to the amino–carboxamido–dithiolato coordination environment in the first coordination sphere of the NiSOD active site, the hydrogen bonds in the second coordination sphere around the NiSOD active center (located between carboxamido carbonyl oxygen of peptide backbone and water molecules and between thiolato sulfurs of cysteine residues and NH protons of the main chain) may be required for tuning the redox potential of metal center.

Coordination Dynamics of Axial Imidazole(s) to Complex 1 in the Ni(II) and Ni(III) States. Complex 1 has an electronic absorption maximum at 449 nm (ϵ 346/M⁻¹ cm⁻¹) in a 4:1 mixture of acetone and DMF (Figure 6A). This feature does not change, even with addition of 1000 equiv of 1-methylimidazole (Figure 6B). This indicates that 1-methylimidazole does not coordinate to the Ni(II) ion of complex 1. We investigated the possibility of coordination of 1-

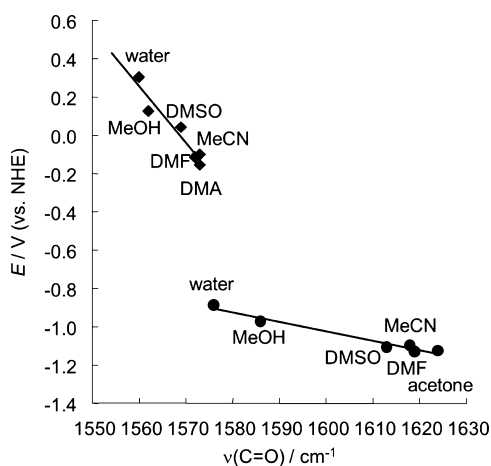


Figure 5. Relationships of E_{pa} (1, ◆) for Ni(II)/(III) and $E_{1/2}$ (2, ●) for Ni(I)/(II) vs $\nu(\text{C}=\text{O})$ values in several solvents.

Table 5. Relationship between Thiolato Oxidation Potentials of 1 (E_{pa} (S)) and Acceptor Numbers of Solvents

solvent	DMA	DMF	MeCN	DMSO	EtOH	MeOH
AN	13.6	16.0	18.9	19.3	37.1	41.3
$E_{pa}(\text{S})/\text{V}$	0.29	0.30	0.36	0.36	0.44	0.51

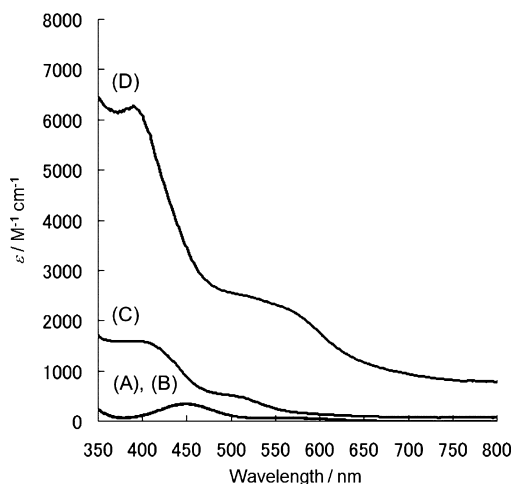


Figure 6. Absorption spectra of (A) Ni(II) complex 1, (B) Ni(II) complex 1 in the presence of 1000 equiv of 1-methylimidazole, (C) Ni(III) complex obtained in the reaction of Ni(II) complex 1 with 1 equiv of FcPF_6 , and (D) the oxidized Ni(III) complex in the presence of 10 equiv of 1-methylimidazole. An acetone/DMF (4:1 v/v) mixture was used as the solvent. Spectra (A) and (B) were measured at room temperature. Spectra (C) and (D) were obtained at -60°C .

methylimidazole to the Ni(III) ion of the oxidized complex 1. Upon oxidation of complex 1 to the Ni(III) state by addition of 1 equiv of ferrocenium hexafluorophosphate (FcPF_6) at -60

Table 4. Relationships between E_{pa} (Ni(II)/(III)) and $\nu(\text{C}=\text{O})$ Values for 1 and between $E_{1/2}$ (Ni(I)/(II)) and $\nu(\text{C}=\text{O})$ Values for 2 in Several Solvents

complex	solvent	acetone	DMA	DMF	MeCN	DMSO	EtOH	MeOH	H ₂ O
1	$\nu(\text{C}=\text{O}), \text{cm}^{-1}$		1573	1572	1573	1569	1562	1560	1554
	E_{pa}, V		-0.181	-0.156	-0.114	-0.103	0.041	0.125	0.303
2	$\nu(\text{C}=\text{O}), \text{cm}^{-1}$	1624		1619	1618	1613		1586	1576
	$E_{1/2}, \text{V}$	-1.127		-1.132	-1.098	-1.107		-0.974	-0.887

$^{\circ}\text{C}$, absorption maxima are observed at 400 nm (1600) and ~ 500 nm (520), which are assigned to $\text{N/O}(\sigma) \rightarrow \text{Ni}(\text{d}x^2-y^2)$ and $\text{S/N/O}(\pi) \rightarrow \text{Ni}(\sigma)$ transitions, respectively (Figure 6C).¹² This absorption spectrum undergoes changes that include appearance of absorption maxima at 393 nm (6200) and 575 nm (2100) when 10 equiv of 1-methylimidazole are added to the solution at -60 $^{\circ}\text{C}$ (Figure 6D). To estimate the structure of the oxidized complex **1**, we carried out EPR spectral studies of the oxidized state of complex **1**. This species exhibits rhombic EPR signals at $g_x = 2.26$, $g_y = 2.19$, and $g_z = 2.01$ (Figure 7A), which are characteristic of a square-planar

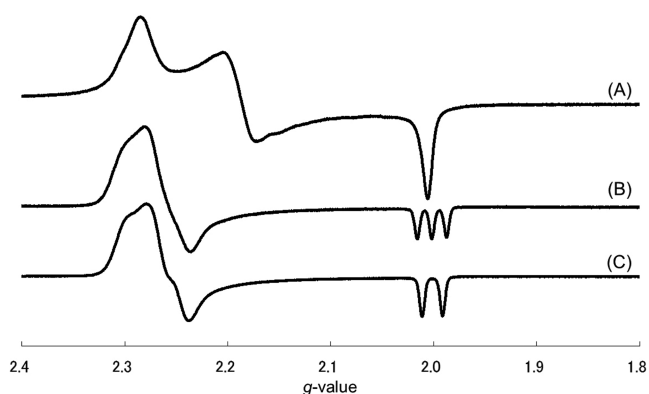


Figure 7. X-band EPR spectra of Ni(III) complex **1** obtained using FcPF_6 as oxidizing reagent (A) in the absence of imidazole ($g = 2.26, 2.19, 2.01$), (B) in the presence of 10 equiv of imidazole ($g = 2.31, 2.26, 2.01$, $|a_N| = 2.5$ mT), and (C) in the presence of 10 equiv of ^{15}N -labeled imidazole ($g = 2.31, 2.26, 2.01$, $|a_N| = 3.2$ mT). All samples were prepared as 5 mM solutions in a 4:1 mixture of acetone/DMF at -78 $^{\circ}\text{C}$ and measured at -196 $^{\circ}\text{C}$.

Ni(III) complex with a N_2S_2 -type ligand.^{9,56,57} When 10 equiv of imidazole are added, the EPR spectrum changes, and signals appear at $g_x = 2.31$, $g_y = 2.26$, and $g_z = 2.01$, $|a_N| = 2.5$ mT (Figure 7B). Interestingly, the g_z signal changes from singlet to triplet splitting upon addition of imidazole. This triplet splitting is very similar to the triplet hyperfine splitting observed for native NiSOD, $g_x = 2.30$, $g_y = 2.22$, and $g_z = 2.01$, $|a_N| = 2.5$ mT.^{3,6} The triplet signal is converted to a doublet ($|a_N| = 3.2$ mT) when ^{15}N -labeled imidazole is added instead of ^{14}N imidazole (Figure 7C). This EPR behavior provides a strong indication that the nitrogen atom of imidazole coordinates to the axial position of the Ni(III) center. These features relating to binding behaviors of imidazole and its derivatives to the Ni(III) center of the oxidized complex **1** are very similar to the coordination features observed for NiSOD.^{6,7}

Reactivity of Ni(II) Complex **1** with Superoxide to Model the NiSOD-catalyzed Reduction of Superoxide.

To investigate the reactivity between Ni(II) complex **1** and superoxide anion, the reaction was monitored by UV-vis and EPR spectroscopies. The UV-vis spectrum of the reaction products produced by the reaction between complex **1** and the same equivalent of KO_2 led to an increase in the absorption intensities of the bands located near 425 and 525 nm and also led to the appearance of a new peak near 650 nm (Figure 8A,B). These absorption features are very similar to those of the end-on Ni(II)-superoxo species reported previously.⁵⁸ The resonance Raman spectrum of the product excited at 532 nm showed Raman band at 1020 cm^{-1} , and an additional peak appeared at 986 cm^{-1} when a mixture of $\text{K}^{16}\text{O}_2/\text{K}^{18}\text{O}_2$ was

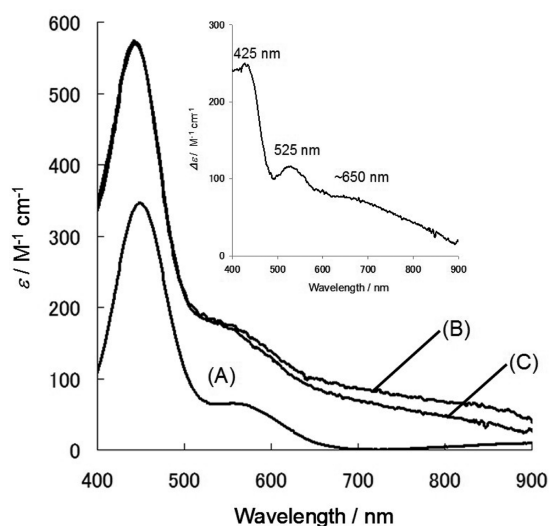


Figure 8. Absorption spectra of (A) Ni(II) complex **1**, (B) Ni(II) complex **1** treated with 1 equiv of KO_2 , (C) Ni(II) complex **1** treated with 1 equiv of KO_2 in the presence of 10 equiv of 1-methylimidazole. (inset) Difference spectrum between spectra (A) and (B). All samples were prepared in a mixed solution of acetone and DMF (4:1) and measured at -60 $^{\circ}\text{C}$. KO_2 was added as a 4 mM solution in DMF. 18-crown-6-ether was used for dissolution of KO_2 .

used instead of K^{16}O_2 (Supporting Information, Figure S4). These Raman bands and isotope shift (-34 cm^{-1}) are consistent with those of end-on Ni(II)-superoxo species.⁵⁸ In EPR spectra observed during the same reaction, the $g_{//}$ value of metal-free superoxide anion at 2.10 is shifted to 2.21 (Figure 9A,B). No other signals were observed in the low magnetic field

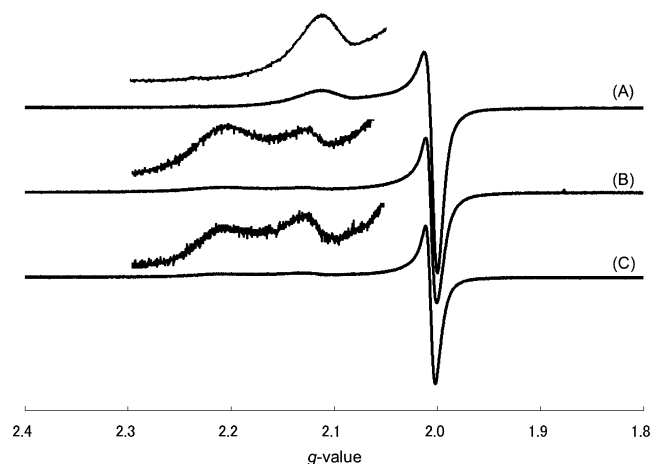


Figure 9. EPR spectra of (A) KO_2 dissolved using 18-crown-6-ether in DMF ($g_{//} = 2.10$, $g_{\perp} = 2.01$), (B) reaction product of Ni(II) complex **1** treated with KO_2 ($g = 2.21, 2.13, 2.01$), and (C) reaction product of Ni(II) complex **1** treated with KO_2 in the presence of 10 equiv of 1-methylimidazole ($g = 2.21, 2.13, 2.01$). A 4:1 mixture of acetone/DMF was used as the solvent for measurements of (B) and (C). All spectra were obtained at -196 $^{\circ}\text{C}$.

region even at low temperature measurement (4 K, Supporting Information, Figure S5). This EPR spectral change also indicates that the Ni(II) complex **1** interacts with superoxide anion to form a low-spin Ni(II)-superoxo species. The UV-vis and EPR spectral features were observed even when the reaction was carried out in the presence of 10 equiv of 1-

methylimidazole (Figure 8C, Figure 9C). This spectroscopic behavior suggests that Ni(II) complex **1** reacts with superoxide anion to form a Ni(II)-superoxo species and that only superoxide anion binds to the Ni(II) center of complex **1** even in the presence of 1-methylimidazole.

Theoretical Study of the Ni(II) Complex 1-Superoxo Species. To characterize the coordination of superoxide anion to the Ni(II) species of complex **1** and the lower-energy shift in the $g_{//}$ value of superoxo species, we performed a theoretical study of the Ni(II) complex **1** and its superoxo adduct. The optimized structure of complex **1** (Supporting Information, Figure S6) was almost the same as its X-ray structure. For the optimization of Ni(II)-superoxo species, the superoxide-binding low-spin Ni(II) species was employed based on the results of resonance Raman and EPR spectroscopic behaviors. The optimized structure is shown in Figure 10A. As a result of

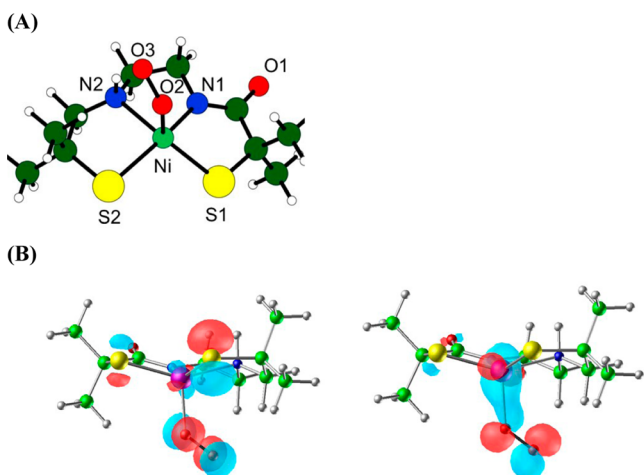


Figure 10. Optimized structure (A) and the π^*_x (B, left) and π^*_y orbitals (B, right) of the Ni(II)-superoxo adduct obtained in the reaction between Ni(II) complex **1** and KO_2 . Selected bond lengths (Å) and angles (deg): Ni–N(1) = 1.994, Ni–N(2) = 2.172, Ni–S(1) = 2.319, Ni–S(2) = 2.391, Ni–O(2) = 1.941, O(2)–O(3) = 1.333, N(2)–O(3) = 2.782, N(1)–Ni–S(2) = 144.20, N(2)–Ni–S(1) = 158.93, N(1)–Ni–S(1) = 84.07, S(1)–Ni–S(2) = 100.46, N(2)–Ni–S(2) = 82.94, N(1)–Ni–N(2) = 81.40, N(1)–Ni–O(2) = 101.71, N(2)–Ni–O(2) = 86.57, S(1)–Ni–O(2) = 111.37, S(2)–Ni–O(2) = 109.25, Ni–O(2)–O(3) = 123.97.

binding of superoxide anion, the Ni–N and Ni–S bonds of Ni(II) complex **1** are elongated from 1.845 and 1.930 Å to 1.994 and 2.172 Å and from 2.148 and 2.198 Å to 2.319 and 2.391 Å, respectively. These significant bond elongations are likely induced by the decrease in Lewis acidity of the Ni(II) center upon coordination of superoxide anion. The optimized structure of the Ni(II)-superoxo adduct is square-pyramidal with a superoxide anion at the axial position of the Ni(II) center. The O(2)–O(3) bond length of the coordinated superoxide (1.333 Å) is consistent with that of the Ni(II)-superoxo species (1.34 Å),⁵⁸ although it is a side-on structure. Interestingly, the proximal oxygen of the bound superoxide anion is directed toward the amino nitrogen (N2) and interacts with the amino hydrogen; the N(2)⋯O(3) distance is 2.782 Å, and the N(2)–H–O(3) angle is 145.06°. The stability of the superoxo species dramatically decreases when the superoxide anion bound to the opposite side of the Ni(II) complex does not form such a hydrogen bond (+26.54 kJ/mol).

As mentioned previously, the EPR study revealed that the $g_{//}$ value of superoxide anion shifts to a lower-energy region from 2.10 to 2.21 upon coordination of superoxide anion to the Ni(II) center of complex **1**. Other EPR investigations of the superoxide anion bound to the metal complexes have indicated that the $g_{//}$ values of the bound superoxo moiety shift to a higher-energy region upon interaction with a metal ion.^{58–60} For the Ni(II)-superoxo complexes, two such studies have been reported.^{61,62} The EPR signals are rhombic although the g values are found in a lower-energy region. However, in our case, the signals are axial although the $g_{//}$ values shift to a lower-energy region. The $g_{//}$ value of superoxide anion generally depends on the energy gap between π^*_x and π^*_y orbitals of the superoxide anion; a smaller energy gap gives a larger $g_{//}$ value, while a larger energy gap gives a smaller value.⁶³ On the basis of the DFT calculation described above, we provide an estimation of the energy gap between the π^*_x and π^*_y orbitals of the superoxide anion bound to the Ni(II) center of complex **1**. This estimated energy gap is 0.29 eV, which is smaller than that of the metal-free superoxide anion (1.07 eV). This result is consistent with the EPR spectral behavior observed upon coordination of superoxide anion to the Ni(II) center of complex **1**.

Reactivity of the Ni(II)-Superoxo Species with a Proton in the Presence/Absence of 1-Methylimidazole.

To investigate the reactivity of the Ni(II)-superoxo species with a proton, we added 2,6-dimethylpyridinium trifluoromethanesulfonate as the proton source to the complex **1**-superoxo species in the presence/absence of 1-methylimidazole. Interestingly, different EPR spectral behavior was observed depending on the presence or absence of 1-methylimidazole. In the absence of 1-methylimidazole, the Ni(II)-superoxo species is EPR silent (Figure 11B) upon addition of the proton source. This suggests that the superoxide anion bound to the Ni(II) center undergoes disproportionation without electron transfer. On the other hand, when the proton source is added to the Ni(II) complex **1**-superoxo species in the presence of 10 equiv of 1-methylimidazole, a characteristic EPR spectrum appears (Figure 11C). This spectrum indicates a low-spin Ni(III) species with 1-methylimidazole at the axial position, because the triplet peak at $g = 2.01$ arises from binding of the 1-methylimidazole nitrogen ($I_N = 1$). This EPR spectrum is similar to that of the Ni(III) species that was obtained by the oxidation of Ni(II) complex **1** using FcPF_6 in the presence of 10 equiv of 1-methylimidazole (Figure 11D). This EPR spectral behavior indicates that the resulting species is the Ni(III) complex with 1-methylimidazole at the axial position, and the structural/electrochemical dynamics correspond to the superoxide-reducing step of NiSOD. These findings strongly suggest that the presence of a proton source and coordination of histidine to the Ni(III) center are both necessary in the superoxide-reduction step of NiSOD.

Reactivity of the Ni(III) Complex with a Superoxo Anion As a Model of the Superoxo-Oxidizing Step.

To understand the superoxide-oxidizing step of NiSOD, 0.8 equiv of KO_2 was added to the Ni(III) complex with 1-methylimidazole at the axial position. This Ni(III) species was prepared by oxidation of Ni(II) complex **1** using FcPF_6 as an oxidizing reagent (Figure 11D). After the reaction, the EPR signal is weakened (Figure 11E). This indicates that the Ni(III) center was reduced to the Ni(II) state by the superoxide anion. However, we cannot speculate from this study whether this reaction is a through-space reaction or a through-bond reaction.

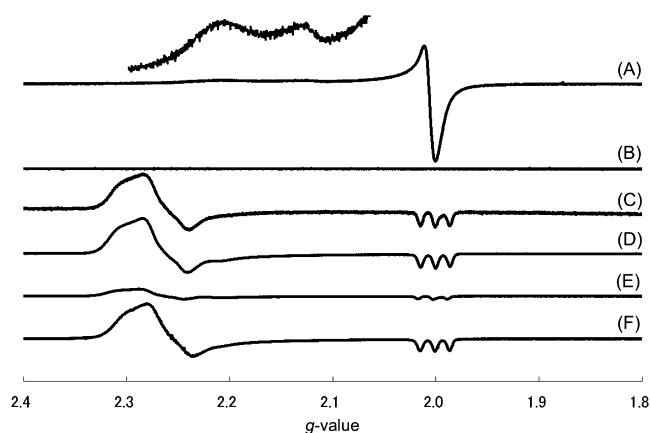


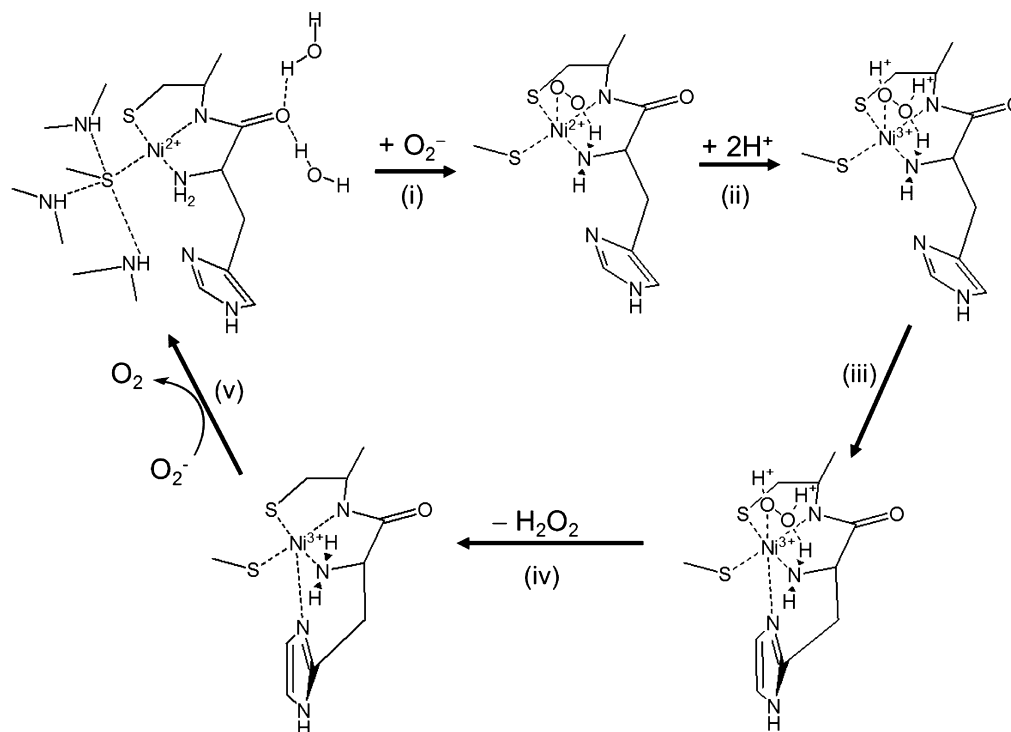
Figure 11. EPR spectra obtained (A) by the reaction of Ni(II) complex **1** with KO_2 ($g = 2.21, 2.13, 2.01$), (B) by the addition of 2,6-dimethylpyridinium trifluoromethanesulfonate (10 equiv) as a proton source for the reaction product of Ni(II) complex **1** and KO_2 in absence of 1-methylimidazole, (C) by the addition of 2,6-dimethylpyridinium trifluoromethanesulfonate (10 equiv) as a proton source to the reaction product of Ni(II) complex **1** and KO_2 in the presence of 1-methylimidazole (10 equiv) ($g = 2.26, 2.19, 2.01$, $|A| = 2.5$ mT), (D) by the reaction of Ni(II) complex **1** with FcPF_6 in the presence of 1-methylimidazole (10 equiv) ($g = 2.26, 2.19, 2.01$, $|A| = 2.5$ mT), (E) by the addition of KO_2 (0.8 equiv) to the Ni(III) complex with 1-methylimidazole, which was obtained in the reaction between Ni(II) complex **1** and FcPF_6 in the presence of 1-methylimidazole (10 equiv), and (F) by the addition of 100 equiv of $(n\text{-Bu})_4\text{N N}_3$ to the imidazole-binding Ni(III) complex ($g = 2.26, 2.19, 2.01$, $|A| = 2.5$ mT). All samples were prepared as 4 mM solutions of a 4:1 mixture of acetone/DMF, and all EPR spectra were measured at -196 °C.

We therefore conducted the Ni(III) ion binding model reaction using azide anion instead of superoxide anion. Azide has a $\text{p}K_a$

value similar to that of the superoxide anion (O_2^- : 4.88, N_3^- : 4.65), and binding to Ni(III) is not accompanied by the redox reaction. However, addition of large excess amounts of N_3^- anion (100 equiv) to the 1-methylimidazole-coordinated Ni(III) species does not produce EPR spectral changes (Figure 11F). This suggests that the superoxide anion cannot bind to the Ni(III) species. Judging from this EPR spectral behavior, we conclude that the superoxide-oxidizing step of NiSOD depends upon electron transfer from superoxide anion to the Ni(III) species via a through-space mechanism without coordination of superoxide anion.

Proposed Mechanism of Superoxide-Reducing/Oxidizing Steps for NiSOD. The above-mentioned oxidation and reduction behavior observed in the reaction with KO_2 using complex **1** corresponds to the superoxide-reducing and -oxidizing steps of NiSOD, respectively. We therefore propose the following superoxide dismutation mechanism for NiSOD (shown in Scheme 2): (i) A superoxide anion binds to the Ni(II) center at the axial position in the end-on fashion, in which the terminal oxygen of the superoxide anion is directed to the amino hydrogen of the terminal histidine to form a hydrogen bond with its NH proton; (ii) two protons interact with the superoxide anion bound to the Ni(II) center, and this promotes transfer of an electron from the Ni(II) center to the superoxide anion; (iii) the imidazole group of the terminal histidine coordinates to the axial position of the oxidized Ni(III) center; (iv) the reduced peroxide leaves the active site as H_2O_2 ; (v) a second superoxide anion is drawn to the Ni(III) ion by electrostatic attraction, and this second superoxide anion is oxidized in a through-space electron transfer reaction and is released as a dioxygen molecule. Judging from the azide coordination behavior to the model Ni(III) center with 1-methylimidazole at the axial position, the superoxide anion may be oxidized without coordinating to the Ni(III) center. This

Scheme 2. Proposed Superoxide Reduction/Oxidation Mechanisms in NiSOD



proposed mechanism is supported by the fact that the metal center of NiSOD has a higher redox potential (+0.29 V vs NHE)⁵⁵ than that of superoxide anion under aqueous conditions (−0.16 V vs NHE).¹¹ This higher redox potential is induced by the hydrogen bonds between the carboxamido oxygen and water molecules and between the thiolato sulfur of Cys6 residue and NH protons of the peptide backbone.

CONCLUSION

To gain an understanding of the mechanism of disproportionation of superoxide anion by NiSOD, we designed and prepared a novel square-planar Ni(II) complex **1** with an amino–carboxamido–dithiolato-type ligand (L_1) as a model compound of the NiSOD active site. This model has the same functional groups as the active center of NiSOD enzyme. Ni(II) complex **1** retains a square-planar structure in all solvents employed in this study and interacts with solvent molecules at the carboxamido oxygen and thiolato sulfurs. The redox potential for the Ni(II)/(III) process of **1** is dramatically affected by the attractive interactions. Complex **1** in water has essentially the same redox potential value as that of native NiSOD. Imidazole and its derivatives coordinate to the oxidized Ni(III) complex **1** at the axial position of the metal center but not to the Ni(II) species. This coordination behavior is quite similar to that of NiSOD. We also investigated the reaction between the Ni(II) complex **1** and superoxide anion and the axial coordination behavior of 1-methylimidazole to the oxidized Ni(III) complex. In the superoxide-reducing step, coordination of a superoxide anion to the Ni(II) center of complex **1** was demonstrated. We propose that the axial coordination of imidazole to the Ni(III) center and the presence of protons are both necessary for generation of hydrogen peroxide. The interaction of the superoxide anion bound to the Ni(II) center of complex **1** with protons promotes electron transfer from the Ni(II) center to the bound superoxide anion. The Ni(III) complex with 1-methylimidazole at the axial position is reduced to the Ni(II) state by through-space electron transfer from the superoxide anion. This reaction has characteristics similar to those of the superoxide-oxidizing step in NiSOD. In this reaction, the Ni(III) species with 1-methylimidazole at the axial site does not react with azide anion. This suggests that the superoxide anion does not bind to the Ni(III) center in the superoxide-oxidizing step.

According to these findings, we can conclude that the redox potential of the metal center of NiSOD is tuned for SOD function by the presence of hydrogen bonds between the carboxamido oxygen and water molecules and between the thiolato sulfur of Cys6 and an NH proton of the peptide backbone. We also propose that a superoxide anion binds to the Ni(II) center of the NiSOD active site in the superoxide-reducing step, and in the superoxide-oxidizing step, a superoxide anion is oxidized without coordinating to the Ni(III) center.

ASSOCIATED CONTENT

Supporting Information

Synthetic scheme of the Ni(II) complex **1** (Scheme S1), UV–vis spectra of the Ni(II) complexes **1**, **2**, and **3** (Figure S1), IR spectra of the Ni(II) complexes **1** and **2** in several solvents (Figure S2), cyclic voltammograms of the Ni(II) complexes **1**, **2**, and **3** in several solvents (Figure S3), resonance Raman spectra of the reaction products between **1** and $K^{16}O_2$ and between **1** and $K^{16}O_2/K^{18}O_2$ (Figure S4), low-temperature (4

K) EPR spectrum obtained by the reaction between **1** and KO_2 in wide range (Figure S5), optimized structure of complex **1** (Figure S6), and X-ray crystallographic report of **1**. These materials are available free of charge via the Internet at <http://pubs.acs.org>.

AUTHOR INFORMATION

Corresponding Author

*E-mail: masuda.hideki@nitech.ac.jp. Phone: +81-52-735-5228. Fax: +81-52-735-5209.

Notes

The authors declare no competing financial interest.

ACKNOWLEDGMENTS

We gratefully acknowledge support from a Grant-in-Aid for Scientific Research from the Ministry of Education, Science, Sports and Culture, from the Strategic Young Researcher Overseas Visits Program for Accelerating Brain Circulation, and in part by a grant from the Knowledge Cluster Program. We also acknowledge Mr. T. Suzuki for X-ray crystallographic measurement.

REFERENCES

- (1) Miller, A. F.; Sorkin, D. *Comments Mol. Cell. Biophys.* **1997**, *9*, 1–48.
- (2) Cabelli, D. E.; Riley, D.; Rodriguez, J. A.; Valentine, J. S.; Zhu, H. Chapter 10. In *Biomimetic Oxidations Catalyzed by Transition Metal Complexes*; Meunier, B., Ed.; Imperial College Press: London, 2000.
- (3) Youn, H. D.; Kim, E. J.; Roe, J. H.; Hah, Y. C.; Kang, S. O. *Biochem. J.* **1996**, *318*, 889–896.
- (4) Youn, H. D.; Youn, H.; Lee, J. W.; Yim, Y. I.; Lee, J. K.; Hah, Y. C.; Kang, S. O. *Arch. Biochem. Biophys.* **1996**, *334*, 341–348.
- (5) Palenik, B.; Brahmasha, B.; Larimer, F. W.; Land, M.; Hauser, L.; Chain, P.; Lameredin, J.; Regala, W.; Allen, E. E.; McCarren, J.; Paulsen, I.; Dufresne, A.; Partensky, F.; Webb, E. A.; Waterbury, J. *Nature* **2003**, *424*, 1037–1042.
- (6) Barondeau, D. P.; Kassmann, C. J.; Bruns, C. K.; Tainer, J. A.; Getzoff, E. D. *Biochemistry* **2004**, *43*, 8038–8047.
- (7) Wuerges, J.; Lee, J. W.; Yim, Y. I.; Yim, H. S.; Kang, S. O.; Carugo, K. D. *Proc. Natl. Acad. Sci. U.S.A.* **2004**, *101*, 8569–8574.
- (8) (a) Shearer, J.; Zhao, N. *Inorg. Chem.* **2006**, *45*, 9637–9639. (b) Shearer, J.; Long, L. M. *Inorg. Chem.* **2006**, *45*, 2358–2360.
- (9) Kruger, H.-J.; Peng, G.; Holm, R. H. *Inorg. Chem.* **1991**, *30*, 734–742.
- (10) (a) Hatlevik, O.; Blanksma, M. C.; Mathrubootham, V.; Arif, A. M.; Hegg, E. L. *J. Biol. Inorg. Chem.* **2004**, *9*, 238–246. (b) Mathrubootham, V.; Thomas, J.; Staples, R.; McCracken, J.; Shearer, J.; Hegg, E. L. *Inorg. Chem.* **2010**, *49*, 5393–5406.
- (11) Holm, R. H.; Kennepohl, P.; Solomon, E. I. *Chem. Rev.* **1996**, *2239*–2314.
- (12) (a) Fiedler, A. T.; Bryngelson, P. A.; Maroney, M. J.; Brunold, T. C. *J. Am. Chem. Soc.* **2005**, *127*, 5449–5462. (b) Jhonson, O. E.; Ryan, K. C.; Maroney, M. J.; Brunold, T. C. *J. Biol. Inorg. Chem.* **2010**, *15*, 777–793. (c) Fiedler, A. T.; Brunold, T. C. *Inorg. Chem.* **2007**, *46*, 8511–8523.
- (13) Neupane, K. P.; Shearer, J. *Inorg. Chem.* **2006**, *45*, 10552–10566.
- (14) Krause, M. E.; Glass, A. M.; Jackson, T. A.; Laurence, J. S. *Inorg. Chem.* **2010**, *49*, 362–364.
- (15) Gennari, M.; Orio, M.; Pecaut, J.; Neese, F.; Collomb, M.-N.; Duboc, C. *Inorg. Chem.* **2010**, *49*, 6399–6401.
- (16) Shearer, J.; Neupane, K. P.; Callan, P. E. *Inorg. Chem.* **2009**, *48*, 10560–10571.
- (17) (a) Gale, E. M.; Narendrapurapu, B. S.; Simmonet, A. C.; Schaefer, H. F., III; Harrop, T. C. *Inorg. Chem.* **2010**, *49*, 7080–7096. (b) Gale, E. M.; Patra, A. K.; Harrop, T. C. *Inorg. Chem.* **2009**, *48*,

- 5620–5622. (c) Gale, E. M.; Cowart, D. M.; Scott, R. A.; Harrop, T. C. *Inorg. Chem.* **2011**, *50*, 10460–10471. (d) Gale, E. M.; Simmonett, A. C.; Telsler, J.; Schaefer, H. F.; Harrop, T. C. *Inorg. Chem.* **2011**, *50*, 9216–9218.
- (18) Nakane, D.; Funahashi, Y.; Ozawa, T.; Masuda, H. *Chem. Lett.* **2010**, *39*, 344–346.
- (19) Nakane, D.; Kuwasako, S.; Tsuge, M.; Kubo, M.; Funahashi, Y.; Ozawa, T.; Ogura, T.; Masuda, H. *Chem. Commun.* **2010**, *46*, 2142–2144.
- (20) Shearer, J.; Dehestani, A.; Abanda, F. *Inorg. Chem.* **2008**, *47*, 2649–2660.
- (21) Stenson, P. A.; Board, A.; Marin-Becerra, A.; Blake, A. J.; Davies, E. S.; Wilson, C.; McMaster, J.; Schröder, M. *Chem.—Eur. J.* **2008**, *14*, 2564–2576.
- (22) Pelmeshnikov, V.; Siegbahn, P. E. M. *J. Am. Chem. Soc.* **2006**, *128*, 7466–7475.
- (23) Prabhakar, R.; Morokuma, K.; Musaev, D. G. *J. Comput. Chem.* **2006**, *27*, 1438–1445.
- (24) Neupane, K. P.; Gearty, K.; Francis, A.; Shearer, J. *J. Am. Chem. Soc.* **2007**, *129*, 14605–14618.
- (25) Mullins, C. S.; Grapperhaus, C. A.; Kozłowski, P. M. *J. Biol. Inorg. Chem.* **2006**, *11*, 617–625.
- (26) Broering, E. P.; Truong, P. T.; Gale, E. M.; Harrop, T. C. *Biochemistry* **2013**, *52*, 4–18.
- (27) (a) Szilagy, R. K.; Bryngelson, P. A.; Maroney, M. J.; Hedman, B.; Hodgson, K. O.; Solomon, E. I. *J. Am. Chem. Soc.* **2004**, *126*, 3018–3019. (b) Ryan, K. C.; Johnson, O. E.; Cabelli, D. E.; Brunold, T. C.; Maroney, M. J. *J. Biol. Inorg. Chem.* **2010**, *15*, 795–807.
- (28) Shearer, J. *Angew. Chem., Int. Ed.* **2013**, *52*, 2569–2572.
- (29) (a) Tietze, D.; Breitzke, H.; Imhof, D.; Kothe, E.; Weston, J.; Buntkowsky, G. *Chem.—Eur. J.* **2009**, *15*, 517–523. (b) Tietze, D.; Tischler, M.; Voigt, S.; Imof, D.; Ohlenschläger, O.; Görlach, M.; Buntkowsky, G. *Chem.—Eur. J.* **2010**, *16*, 7572–7578. (c) Tietze, D.; Voigt, S.; Mollenhauer, D.; Tischler, M.; Imhof, D.; Gutmann, T.; Gonzalez, L.; Ohlenschläger, O.; Breitzke, H.; Görlach, M.; Buntkowsky, G. *Angew. Chem., Int. Ed.* **2011**, *50*, 2946–2950.
- (30) (a) Krause, M. E.; Glass, A. M.; Jackson, T. A.; Laurence, J. S. *Inorg. Chem.* **2011**, *50*, 2479–2487. (b) Krause, M. E.; Glass, A. M.; Jackson, T. A.; Laurence, J. S. *Inorg. Chem.* **2013**, *52*, 77–83.
- (31) (a) Mullins, C. S.; Grapperhaus, C. A.; Frye, B. C.; Wood, L. H.; Hay, A. J.; Buchanan, R. M.; Mashuta, M. S. *Inorg. Chem.* **2009**, *48*, 9974–9976. (b) Herdt, D. R.; Grapperhaus, C. A. *Dalton Trans.* **2012**, *41*, 364–366.
- (32) Jenkins, R. M.; Singleton, M. L.; Almaraz, E.; Reibenspies, J. H.; Darenbourg, M. Y. *Inorg. Chem.* **2009**, *48*, 7280–7293.
- (33) Lee, W.-Z.; Chiang, C.-W.; Lin, T.-H.; Kuo, T.-S. *Chem.—Eur. J.* **2012**, *18*, 50–53.
- (34) Mach, R. H.; Kung, H. F. *Org. Mass Spectrom.* **1991**, *26*, 528–530.
- (35) Saigo, K.; Usui, M.; Kikuchi, K.; Shimada, E.; Mukaiyama, T. *Bull. Chem. Soc. Jpn.* **1977**, *50*, 1863–1866.
- (36) Nakane, D.; Funahashi, Y.; Ozawa, T.; Masuda, H. *Trans. Mater. Res. Soc. Jpn.* **2009**, *34*, 513–516.
- (37) Gange, R. R.; Coval, C. A.; Lisensky, G. C. *Inorg. Chem.* **1980**, *19*, 2854–2855.
- (38) Dale, H. H.; Evans, C. L. *J. Physiol.* **1920**, *54*, 167–177.
- (39) Altomare, A.; Cascarano, G.; Giacovazzo, C.; Guagliardi, A.; Burla, M.; Polidori, G.; Camalli, M. *J. Appl. Crystallogr.* **1994**, *27*, 435–436.
- (40) Beurskens, P. T.; Admiraal, G.; Beurskens, G.; Bosman, W. P.; De Gelder, R.; Israel, R.; Smits, J. M. M. *Technical Report of the Crystallography Laboratory*; Radboud University: Nijmegen, The Netherlands, 1999.
- (41) Handy, N. C.; Cohen, A. J. *Mol. Phys.* **2001**, *99*, 403–412.
- (42) Hoe, W.-M.; Cohen, A.; Handy, N. C. *Chem. Phys. Lett.* **2001**, *341*, 319–328.
- (43) (a) Perdew, J. P.; Burke, K.; Ernzerhof, M. *Phys. Rev. Lett.* **1996**, *77*, 3865–3868. (b) Perdew, J. P.; Burke, K.; Ernzerhof, M. *Phys. Rev. Lett.* **1997**, *78*, 1396.
- (44) Abdurahman, A.; Renger, T. *J. Phys. Chem. A* **2009**, *113*, 9202–9209.
- (45) Pierloot, K.; Vancoillie, S. *J. Chem. Phys.* **2008**, *128*, 34104–34114.
- (46) Radoń, M.; Pierloot, K. *J. Phys. Chem. A* **2008**, *112*, 11824–11832.
- (47) Hehre, W. J.; Ditchfield, R.; Pople, J. A. *J. Chem. Phys.* **1972**, *56*, 2257.
- (48) Watchers, A. J. H. *J. Chem. Phys.* **1970**, *52*, 1033.
- (49) Hay, P. J. *J. Chem. Phys.* **1977**, *66*, 4377.
- (50) Clark, T.; Chandrasekhar, J.; Spitznagel, G. W.; Schleyer, P. v. R. *J. Comput. Chem.* **1983**, *4*, 294.
- (51) Frisch, M. J.; Trucks, G. W.; Schlegel, H. B.; Scuseria, G. E.; Robb, M. A.; Cheeseman, J. R.; Scalmani, G.; Barone, V.; Mennucci, B.; Petersson, G. A.; Nakatsuji, H.; Caricato, M.; Li, X.; Hratchian, H. P.; Izmaylov, A. F.; Bloino, J.; Zheng, G.; Sonnenberg, J. L.; Hada, M.; Ehara, M.; Toyota, K.; Fukuda, R.; Hasegawa, J.; Ishida, M.; Nakajima, T.; Honda, Y.; Kitao, O.; Nakai, H.; Vreven, T.; Montgomery, J. A., Jr.; Peralta, J. E.; Ogliaro, F.; Bearpark, M.; Heyd, J. J.; Brothers, E.; Kudin, K. N.; Staroverov, V. N.; Kobayashi, R.; Normand, J.; Raghavachari, K.; Rendell, A.; Burant, J. C.; Iyengar, S. S.; Tomasi, J.; Cossi, M.; Rega, N.; Millam, J. M.; Klene, M.; Knox, J. E.; Cross, J. B.; Bakken, V.; Adamo, C.; Jaramillo, J.; Gomperts, R.; Stratmann, R. E.; Yazyev, O.; Austin, A. J.; Cammi, R.; Pomelli, C.; Ochterski, J. W.; Martin, R. L.; Morokuma, K.; Zakrzewski, V. G.; Voth, G. A.; Salvador, P.; Dannenberg, J. J.; Dapprich, S.; Daniels, A. D.; Farkas, O.; Foresman, J. B.; Ortiz, J. V.; Cioslowski, J.; Fox, D. J. *Gaussian 09, Revision A.02*; Gaussian, Inc.: Wallingford, CT, 2009.
- (52) (a) Wasada, H.; Tsutsui, Y. *Bulletin of the College of General Education*, 32; Nagoya University: Furo, Chikusa, Nagoya, Japan, 1995. (b) Takahashi, I.; Wasada, H.; Tsutsui, Y. *MOVIEW: program representing molecular orbital maps by isosurfaces*; Nagoya University: Nagoya, Japan, 2001.
- (53) Grapperhaus, C. A.; Mullins, C. S.; Kozłowski, P. M.; Mashuta, M. S. *Inorg. Chem.* **2004**, *43*, 2859–2866.
- (54) Mayer, U.; Gutmann, V.; Gerger, W. *Monatsh. Chem.* **1975**, *106*, 1235–1257.
- (55) Herbst, R. W.; Guce, A.; Bryngelson, P. A.; Higgins, K. A.; Ryan, K. C.; Cabelli, D. E.; Garman, S. C.; Maroney, M. J. *Biochemistry* **2009**, *48*, 3354–3369.
- (56) Hanss, J.; Kruger, H.-J. *Angew. Chem., Int. Ed.* **1998**, *37*, 360–361.
- (57) Kruger, H.-J.; Holm, R. H. *Inorg. Chem.* **1987**, *26*, 3645–3647.
- (58) Kieber-Emmons, M. T.; Annaraj, J.; Seo, M. S.; Van Heuvelen, K. M.; Tosha, T.; Kitagawa, T.; Brunold, T. C.; Nam, W.; Riordan, C. G. *J. Am. Chem. Soc.* **2006**, *128*, 14230–14231.
- (59) Fukuzumi, S.; Patz, M.; Suenobu, T.; Kuwahara, Y.; Itoh, S. *J. Am. Chem. Soc.* **1999**, *121*, 1605–1606.
- (60) Fukuzumi, S.; Ohkubo, K. *Chem.—Eur. J.* **2000**, *6*, 4532–4535.
- (61) Yao, S.; Bill, E.; Milsman, C.; Wieghardt, K.; Driess, M. *Angew. Chem., Int. Ed.* **2008**, *47*, 7110–7113.
- (62) Hasegawa, K.; Imamura, T.; Fujimoto, M. *Inorg. Chem.* **1986**, *25*, 2154–2160.
- (63) Kanzig, W.; Cohen, M. H. *Phys. Rev. Lett.* **1959**, *3*, 509–510.